



ELSEVIER

Available online at www.sciencedirect.com

SCIENCE @ DIRECT®

Journal of Crystal Growth 265 (2004) 34–40

JOURNAL OF
**CRYSTAL
GROWTH**

www.elsevier.com/locate/jcrysgro

High-electron-mobility ZnO epilayers grown by plasma-assisted molecular beam epitaxy

Kazuhiro Miyamoto^{a,*}, Michihiro Sano^a, Hiroyuki Kato^a, Takafumi Yao^b

^a *Research and Development Center, Stanley Electric Co., Ltd., 1-3-1 Eda-nishi, Aoba-ku, Yokohama, Kanagawa 225-0014, Japan*

^b *Institute for Materials Research, Tohoku University, 2-1-1 Katahira, Aoba-ku, Sendai, Miyagi 980-8577, Japan*

Received 30 November 2003; accepted 20 January 2004

Communicated by M. Schieber

Abstract

High-electron-mobility ZnO epilayers are grown on *c*-plane sapphire with ZnO/MgO double-buffer layers by plasma-assisted molecular beam epitaxy. Reflection high-energy electron diffraction and transmission electron microscopy analysis showed the growth mode of ZnO buffer layers (LT-ZnO) grown at low temperature significantly affected the structural properties of the ZnO epilayers grown at high temperature, thereby affecting the electrical properties of the epilayers. When LT-ZnO was grown at a high-growth-rate, three-dimensional growth dominated and threading dislocation (TD) density was as high as ca. $1 \times 10^{10} \text{ cm}^{-2}$. By using the low growth rate of LT-ZnO, two-dimensional growth dominated and TD density was reduced by one order of magnitude, down to ca. $2 \times 10^9 \text{ cm}^{-2}$, yielding significantly improved electrical properties of the ZnO epilayers. The highest electron mobility in as-grown undoped ZnO film, $145 \text{ cm}^2 \text{ V}^{-1} \text{ s}^{-1}$, was achieved at room temperature, comparable to the mobility previously reported for high-quality bulk ZnO.

© 2004 Elsevier B.V. All rights reserved.

PACS: 81.15.Hi; 81.05.Dz; 61.10.Kw; 73.61.Ga

Keywords: A1. Dislocation density; A1. Electrical properties of ZnO; B1. LT-ZnO; B1. ZnO; B1. ZnO/MgO double-buffer

1. Introduction

ZnO is a well-known material for n-type oxide semiconductors, and is commonly used for transparent conducting electrodes [1,2], gas sensors, and surface acoustic devices. In the past several years, ZnO-based materials have been attracting increas-

ing attention because of their applicability to UV light-emitting devices owing to the direct band gap of 3.37 eV at room temperature (RT) and a large exciton binding energy of 60 meV. Such high binding energy ensures survival of excitons even at RT, as evidenced by optically pumped room-temperature exciton lasing [3] and high-temperature excitonic stimulated emission [4]. Recently, the growth of high-quality ZnO films on sapphire substrates have been reported by several groups [5–7], where undoped ZnO layers showed

*Corresponding author.

E-mail address: kazuhiro.miyamoto@stanley.co.jp
(K. Miyamoto).

n-type conductivity with typical electron concentration ranging from 2×10^{16} to $5 \times 10^{17} \text{ cm}^{-3}$ and electron mobility of ca. $100 \text{ cm}^2 \text{ V}^{-1} \text{ s}^{-1}$. These values, however, should be compared with electron concentration ($1\text{--}8 \times 10^{16} \text{ cm}^{-3}$) and mobility values ($150\text{--}350 \text{ cm}^2 \text{ V}^{-1} \text{ s}^{-1}$) of high-quality bulk ZnO [8].

Because control of the conductivity of n-type ZnO has been recently achieved [9,10], the remaining material issue required for use of ZnO in the fabrication of optoelectronic devices is p-type doping. Despite several efforts to achieve p-type doping, no reliable results have been reported. The failure to achieve such doping is presumably due to the presence of residual donor-type defects in ZnO epilayers that might counteract the effect of acceptor impurities, thereby making the resultant layer highly resistive. Therefore, the growth of high-quality ZnO layers with minimal residual electron concentration is prerequisite for the growth of p-type ZnO. The origin of residual donor-type impurities and defects is still controversial [11–14]. However, we have suggested that the improvement of electrical properties (i.e. increase in electron mobility and decrease in electron concentration) of undoped ZnO films is due to a decrease in dislocation density (N_{dis}) based on the X-ray diffraction measurements and analysis of electron mobility [15]. Therefore, because formation of donor-type defects is mainly attributed to dislocations, minimizing N_{dis} is critical to realize p-type ZnO. Look et al. [16] recently reported that reproducible N-doped p-type ZnO films can be grown on Li-doped semi-insulating ZnO substrates. This reproducibility is presumably due to a decrease in concentration of residual donor-type defect in ZnO epilayers owing to lattice-matched epitaxy.

In the present paper, we will report the role of a thin MgO buffer layer, the influence of the growth conditions of low-temperature ZnO buffer layers (LT-ZnO) on both electrical and structural properties of high-temperature grown ZnO epilayers (HT-ZnO), and the effect of the dislocations on electron mobility. Results showed that a ZnO film grown at RT had a high electron mobility of $145 \text{ cm}^2 \text{ V}^{-1} \text{ s}^{-1}$, comparable to the mobility in high-quality bulk ZnO.

2. Experimental procedure

ZnO films were grown by a custom-designed plasma-assisted molecular beam epitaxy (P-MBE) system (Vieetech Japan) as shown in Fig. 1. An inductively coupled RF plasma source 13.56 MHz [17] (MPD21, Oxford Applied Research) was used as an oxygen radical source. The 6N oxygen gas was introduced into the plasma gun through a mass flow controller (MFC). The 7N Zn were vaporized by an EPI SUMO cell, and the 6N Mg were vaporized by a conventional effusion cell. The beam flux was measured by either quartz thickness monitor or a nude ion gauge mounted beside the substrate holder. The Zn beam flux was varied from 0.1 to 3.0 A/s for LT-ZnO growth. The growth time of LT-ZnO was varied from 30 s to 35 min. During growth, the RF power of the oxygen plasma source was kept at 160–200 W. The substrate temperature was measured by a thermocouple fixed on the backside of the substrate holder. The *c*-plane sapphire substrates were degreased in 2-propanol, acetone, and then chemically etched in $\text{H}_2\text{SO}_4\text{:H}_3\text{PO}_4 = 3\text{:}1$ at 110°C for 30 min followed by rinsing with deionized water and drying by boiling acetone. Prior to growth, the substrate was annealed at 800°C for 30 min then was treated in atomic hydrogen generated by an EPI atomic hydrogen source to remove adsorbed residual contamination such as hydrocarbons. The typical film growth procedures were as follows.

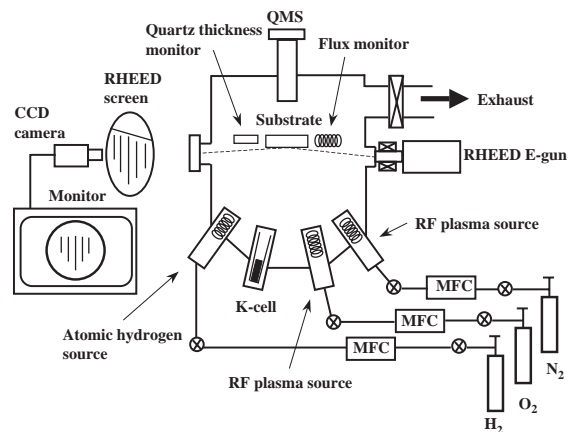


Fig. 1. Schematic diagram of the P-MBE system.

First, a thin MgO buffer layer was grown at 800°C until its reflection high-energy electron diffraction (RHEED) pattern changed from a streaky pattern to a spotty one [5]. Then, an LT-ZnO was grown at 350°C or 500°C. After the LT-ZnO film was annealed at 850°C for 10 min, an undoped ZnO layer (HT-ZnO) was grown at 700°C. The entire growth process was monitored based on RHEED patterns obtained at 20 kV. The total thickness of the ZnO film was measured by a Sloan DECTAK 3030 surface profiler. The HT-ZnO layers were grown for about 4.5 h at a growth rate of about 0.2–0.3 μm/h. Both the Hall mobility and the residual carrier concentration of as-grown ZnO epitaxial films were measured by the van der Pauw method with a magnetic field of 0.485 T at RT (HL5560PC Hall effect measurement system, Bio-Rad Micromeritics). The N_{dis} value was investigated by the transmission electron microscopy (TEM) analysis.

3. Results and discussion

3.1. Role of a thin MgO buffer layer

When c -axis oriented ZnO films are grown on c -plane sapphire, twin defects with a 30° in-plane crystal orientation misalignment (30° rotation domains) easily form [18,19]. These domains must be eliminated to assure high-quality ZnO films. Chen et al. [5] recently reported that inserting a thin MgO buffer layer between a ZnO buffer layer and a c -plane sapphire substrate completely eliminates these 30° rotation domains and significantly reduces N_{dis} . According to the RHEED patterns, the epitaxial relationship is determined as $\text{ZnO}[1\ 1\ \bar{2}\ 0] \parallel \text{MgO}[\bar{1}\ 1\ 0] \parallel \text{sapphire}[1\ \bar{1}\ 0\ 0]$ and $\text{ZnO}[1\ \bar{1}\ 0\ 0] \parallel \text{MgO}[\bar{1}\ \bar{1}\ 2] \parallel \text{sapphire}[1\ 1\ \bar{2}\ 0]$ [5]. The elimination mechanisms of 30° rotation domains are as follows. The MgO buffer layer can partially accommodate the lattice mismatch of 18%, since the in-plane lattice constant of MgO (1 1 1) plane lies just in between ZnO and sapphire. Additionally, the MgO buffer has six-fold coordination and serves as a transition layer from six-fold coordination of sapphire to four-fold coordination of ZnO, which partially accommodates the crystallographic

mismatch. These mismatches should be accommodated by LT-ZnO leading to the formation of interface with reduced interface energy during high temperature annealing after buffer layer deposition. In other words, a thin MgO buffer layer acts as a reducer of the lattice mismatch between ZnO and c -plane sapphire, and this technique can be used for another heteroepitaxy system having a large lattice mismatch such as GaN/ c -sapphire.

3.2. Effects of Zn beam flux in low-temperature ZnO buffer layers growth on electrical properties of high-temperature grown ZnO epilayers

Table 1 shows measured electrical properties (Hall mobility μ and residual carrier concentration n) of as-grown ZnO films at various growth conditions of LT-ZnO. The electrical properties of the ZnO films were significantly improved by reducing Zn beam flux from 3 (high-growth-rate LT-ZnO) to 0.1 A/s (low-growth-rate LT-ZnO). The electrical properties of ZnO films were not affected by the growth temperature of LT-ZnO. Fig. 2 shows RHEED patterns for various growth stages of ZnO films that had a low-growth-rate LT-ZnO. The initial growth stage of a low-growth-rate LT-ZnO was as follows. Spotty patterns of ZnO gradually appear superimposed on the MgO patterns with the rod spacing ca. 9% smaller [5]. The spotty patterns gradually evolved into streaky patterns with 3×3 reconstruction (Figs. 2a and d, where growth time of LT-ZnO = 35 min). After the 10 min annealing, sharp streaky patterns for the low-growth-rate LT-ZnO appeared (Figs. 2b and

Table 1
Measured electrical properties of ZnO films at various growth conditions of LT-ZnO

Zn beam flux (A/s)	Growth temperature of LT-ZnO (°C)	n (cm ⁻³)	μ (cm ² V ⁻¹ s ⁻¹)
3.0	350	5.3×10^{17}	64 ^a
0.1	350	1.4×10^{17}	137
3.0	500	4.9×10^{17}	57
0.1	500	1.6×10^{17}	145 ^b

^{a,b}Specimens for TEM analysis.

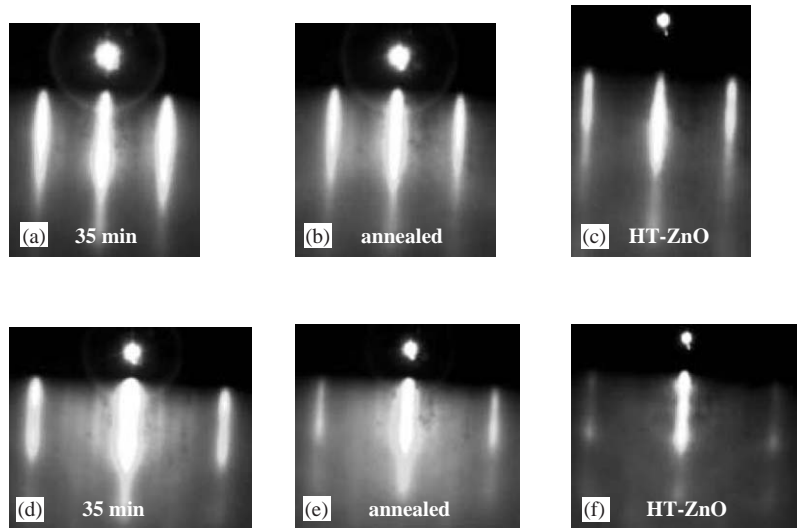


Fig. 2. RHEED patterns at the various growth stage of a ZnO film with a low-growth-rate LT-ZnO. Electron beam azimuth was (a)–(c) ZnO[1 1 2 0] and (d)–(f) ZnO[1 1 0 0].

e), and the streaky patterns remained with continued growth of the HT-ZnO (Figs. 2c and f). In contrast, in the high-growth-rate LT-ZnO, spotty patterns for ZnO appeared after only a few seconds of growth, then the pattern showed diffused spotty streaks (growth time of LT-ZnO = 30 s). Although these patterns sharpened after high temperature annealing, the spotty feature remained, and further growth of HT-ZnO showed no sharp streaky pattern. These observations reveal that the surface morphology of the annealed ZnO buffer strongly affected the growth of HT-ZnO. Chen et al. [20] reported that ZnO epilayers grown under oxygen-rich conditions have atomically flat surfaces. Moreover, Ko et al. [21] reported that an incorporation barrier for O adatoms is smaller than that for Zn adatom during ZnO growth. Therefore, at the initial stage of ZnO buffer growth, the nucleation density depends on the Zn adatom density, that is, lower Zn beam flux (i.e., higher oxygen-rich condition) leads to a lower nucleation density. Thus, lateral growth (i.e. two-dimensional nucleation and growth) of the ZnO buffer is more enhanced by a low-growth-rate LT-ZnO than by a high-growth-rate LT-ZnO, and such lateral growth yields an atomically flat and ordered surface of the ZnO buffer. The

RHEED patterns in Fig. 2 offer evidence to support this explanation. Consequently, the low-growth-rate LT-ZnO provides higher structural quality buffer for HT-ZnO growth, leading to the improved structural and electrical properties of ZnO films.

3.3. Cross-sectional TEM images of ZnO films

In general, the large lattice-mismatched epitaxial growth leads to a high density of threading dislocations (TDs) in epilayers; for example, N_{dis} of GaN/sapphire typically ranges between 10^9 and 10^{11} cm^{-2} [22] and that of ZnO/sapphire between 10^9 and 10^{10} cm^{-2} [23]. N_{dis} as low as 10^6 – 10^7 cm^{-2} has been achieved in a GaN/sapphire system by epitaxial lateral overgrowth or by GaN/AlN low-temperature-grown inter layers [24–26]. Ng et al. [27] reported that edge-type TDs degrade the electrical properties of GaN films. Therefore, electrical properties of ZnO films should improve by decreasing edge-type TDs. The effects of low-growth-rate LT-ZnO on the structural properties of ZnO films were clearly evident in cross-sectional TEM images of two-type ZnO films: a ZnO film with a high-growth-rate LT-ZnO (sample a in Table 1, and Figs. 3a and b), and a ZnO film with

a low-growth-rate LT-ZnO (sample b in Table 1 and Figs. 3c and d). Figs. 3a–d show $1\text{ g}/3\text{ g}$ weak beam dark field cross-sectional TEM images of the ZnO films. In the ZnO film with a high-growth-rate LT-ZnO, so many edge dislocations were detected (estimated at 70 TDs in the region shown in Fig. 3a), that not all could be labeled by an open triangle in the figure, whereas no screw or mixed dislocations were detected (Fig. 3b). The estimated dislocation density of each component in the ZnO film with a high-growth-rate LT-ZnO was $N_{\text{dis}(\text{edge})} = 1 \times 10^{10}\text{ cm}^{-2}$, $N_{\text{dis}(\text{screw})} = 0$, and $N_{\text{dis}(\text{mixed})} = 0$. In the ZnO film with a low-growth-rate LT-ZnO, the majority of the dislocations were edge type, with a few screw and mixed dislocations. The estimated dislocation density of each component in the ZnO film with a low-growth-rate LT-ZnO was $N_{\text{dis}(\text{edge})} = 1.3 \times 10^9\text{ cm}^{-2}$, $N_{\text{dis}(\text{screw})} = 1.3 \times 10^8\text{ cm}^{-2}$ and $N_{\text{dis}(\text{mixed})} = 5.4 \times 10^8\text{ cm}^{-2}$. In both films, the majority of TDs running along the c -axis direction were edge dislocations [28]. The estimated total dislocation density $N_{\text{dis}(\text{total})}$ of the ZnO film with a high-growth-rate LT-ZnO was $1 \times 10^{10}\text{ cm}^{-2}$ and that of ZnO film with a low-growth-rate LT-ZnO was $2 \times 10^9\text{ cm}^{-2}$. These observations suggest that the electrical properties of ZnO films can be improved mainly by decreasing the edge dislocations by introducing a low-growth-rate LT-ZnO, and that the density of screw

and mixed dislocations is so low that they have little effect on the electrical properties of ZnO films.

3.4. Electrical properties of high-temperature grown ZnO epilayers

The effect of dislocations on electron mobility was clarified by analyzing the mobility taking five scattering mechanisms into account: ionized impurity scattering (μ_{ii}), piezoelectric scattering (μ_{pe}), deformation potential scattering (μ_{def}), polar optical phonon scattering (μ_{pop}), and dislocation scattering (μ_{dis}). Details of the scattering mechanisms have been described elsewhere [15]. Fig. 4 shows the calculated electron mobility of ZnO as a function of electron concentration with and without dislocation scattering (dashed and solid lines, respectively) at RT. To investigate whether the dominant impurities act as donors or acceptors in ZnO films, depth profile was measured using secondary ion mass spectroscopy (SIMS). Based on the resultant depth profile (Fig. 5), the estimated impurity concentrations in the ZnO film with a low-growth-rate LT-ZnO were $[\text{Al}] = 2 \times 10^{16}\text{ cm}^{-3}$, $[\text{Si}] = 4 \times 10^{15}\text{ cm}^{-3}$, $[\text{Na}] = 2 \times 10^{14}\text{ cm}^{-3}$, and $[\text{K}] = 2 \times 10^{13}\text{ cm}^{-3}$, and those in the ZnO film with a high-growth-rate LT-ZnO were $[\text{Al}] = 2 \times 10^{17}\text{ cm}^{-3}$, $[\text{Si}] = 4 \times 10^{16}\text{ cm}^{-3}$, $[\text{Na}] = 4 \times 10^{14}\text{ cm}^{-3}$, and

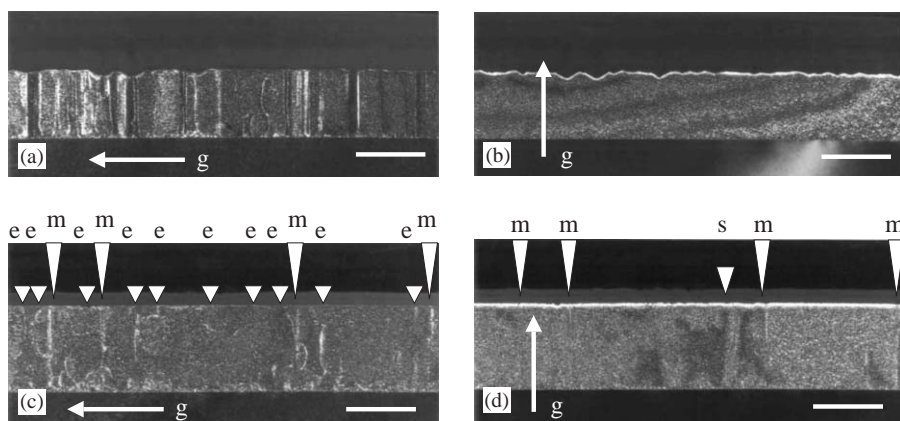


Fig. 3. Dislocations in ZnO films with (a, b) ZnO film with a high-growth-rate LT-ZnO and (c, d) ZnO film with a low-growth-rate LT-ZnO revealed by $1\text{ g}/3\text{ g}$ weak-beam dark-field cross-sectional TEM images with (a) $g = [1\ \bar{1}\ 0\ 0]$, (b) $g = [0\ 0\ 0\ 2]$, (c) $g = [1\ \bar{1}\ 0\ 0]$, and (d) $g = [0\ 0\ 0\ 2]$. Letters e, m, and s indicate edge, mixed, and screw dislocations, respectively. Thickness of specimens along electron beam azimuth was about $0.13\ \mu\text{m}$. Scale bar represents $1\ \mu\text{m}$.

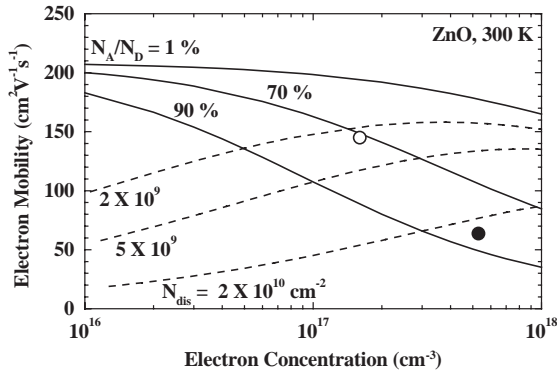


Fig. 4. Electron mobility as a function of electron concentration. Solid lines show the calculated electron mobilities without dislocation scattering at various compensation ratios (N_A/N_D). Dashed lines show the calculated electron mobilities with dislocation scattering for different dislocation densities (N_{dis}). ○, estimated $N_{\text{dis}}(\text{total}) = 2 \times 10^9 \text{ cm}^{-2}$ and ●, estimated $N_{\text{dis}}(\text{total}) = 1 \times 10^{10} \text{ cm}^{-2}$.

$[K] = 8 \times 10^{12} \text{ cm}^{-3}$. These impurities come from the quartz discharge tube of the O_2 plasma source. At a 100% ionization rate of both donor (Al) and acceptors (Na and K), the compensation ratio (N_A/N_D) should be 1%. However, the calculated electron mobility for N_A/N_D of 1% without dislocation scattering was much higher than the measured Hall mobility. Although the measured mobilities for $N_A/N_D = 70$ and 90% were curve-fitted (solid lines in Fig. 4), some discrepancy between the fitted and measured values was evident. This discrepancy indicates that another scattering mechanism is needed to explain Fig. 4. We therefore calculated the electron mobility by using dislocation scattering. The $N_{\text{dis}}(\text{total})$ estimated based on TEM analysis were curve-fitted (dashed lines in Fig. 4). Similar results were reported for GaN/sapphire system that had a large lattice mismatch [22,27]. Moreover, Read [29] suggested that edge dislocations can introduce acceptor centers (dangling bonds) along the dislocation line and therefore can capture electrons from the conduction band of an n-type semiconductor. The dislocation line becomes negatively charged, and a space charge is formed around it, which scatters electrons and thus reduces their mobility. We conclude that the dominant electron scattering mechanism was dislocation scattering,

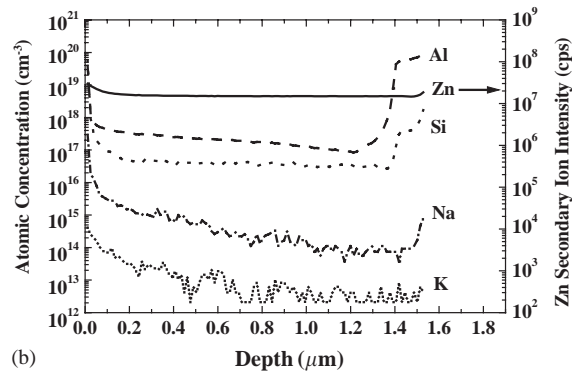
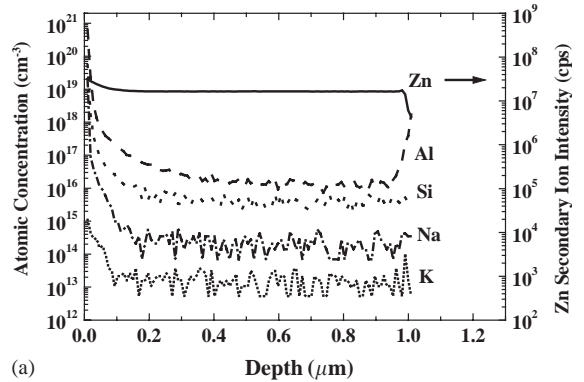


Fig. 5. SIMS depth profile of a typical ZnO film with (a) a low-growth-rate LT-ZnO and (b) a high-growth-rate LT-ZnO. Measured residual carrier concentration of a ZnO film with a low-growth-rate LT-ZnO was $1.6 \times 10^{17} \text{ cm}^{-3}$ and that of a ZnO film with a high-growth-rate LT-ZnO was $5.3 \times 10^{17} \text{ cm}^{-3}$.

and that both the increase in electron mobility up to $145 \text{ cm}^2 \text{ V}^{-1} \text{ s}^{-1}$ and the decrease in electron concentration down to $1.6 \times 10^{17} \text{ cm}^{-3}$ are due to a decrease in dislocation density. However, the electron concentration is still limited at about $1 \times 10^{17} \text{ cm}^{-3}$. If a 100% ionization rate of unintentionally doped impurities is assumed, the estimated residual carrier (electron) concentration in a ZnO film with a low-growth-rate LT-ZnO is $2.0 \times 10^{16} \text{ cm}^{-3}$ and that of a ZnO film with a high-growth-rate LT-ZnO is $2.0 \times 10^{17} \text{ cm}^{-3}$, based on the SIMS observations. The measured residual carrier concentrations, however, are considerably larger, namely, $1.6 \times 10^{17} \text{ cm}^{-3}$ in the ZnO film with a low-growth-rate LT-ZnO and $5.3 \times 10^{17} \text{ cm}^{-3}$ in the ZnO film with a high-growth-rate LT-ZnO. Therefore, residual donors

should be considered, such as zinc interstitial [11], oxygen vacancy [13,14], and hydrogen [12]. Sano et al. [30] recently found that hydrogen irradiation during ZnO growth leads to higher structural quality ZnO films with smaller residual carrier concentration, suggesting that hydrogen does not act as a dominant donor. Moreover, low structural quality ZnO films such as polycrystalline films have very high electron concentration [1]. The predominant origin of residual donors apparently is native donors such as zinc interstitial and/or oxygen vacancy, the formation of which is generated by dislocations.

4. Conclusions

In conclusion, we have demonstrated the growth of high-quality ZnO films by using a low-growth-rate LT-ZnO. Both TEM and calculated electron mobilities revealed that the improvement in the electrical properties of these ZnO films is due to a decrease in dislocation density. The highest electron mobility of $145 \text{ cm}^2 \text{ V}^{-1} \text{ s}^{-1}$ in as-grown ZnO film was achieved at RT and is comparable with that in high-quality bulk ZnO [8]. However, the electron concentration is still limited at about $1 \times 10^{17} \text{ cm}^{-3}$. To realize p-type ZnO/sapphire, a lower dislocation density will be needed.

Acknowledgements

We gratefully acknowledge Drs. Y.F. Chen, H.J. Ko, and S.K. Hong for valuable discussions.

References

- [1] K. Miyamoto, M. Yoshida, H. Toyotama, S. Onari, T. Arai, *Jpn. J. Appl. Phys.* 30 (1991) 1830.
- [2] H. Hirasawa, M. Yoshida, S. Nakamura, Y. Suzuki, S. Okada, K. Kondo, *Sol. Energy Mater. Sol. Cells* 67 (2001) 231.
- [3] D.M. Bagnall, Y.F. Chen, Z. Zhu, T. Yao, S. Koyama, M.Y. Shen, T. Goto, *Appl. Phys. Lett.* 70 (1997) 2230.
- [4] D.M. Bagnall, Y.F. Chen, Z. Zhu, T. Yao, M.Y. Shen, T. Goto, *Appl. Phys. Lett.* 73 (1998) 1038.
- [5] Y.F. Chen, H.J. Ko, S.K. Hong, T. Yao, *Appl. Phys. Lett.* 76 (2000) 559.
- [6] K. Iwata, P. Fons, S. Niki, A. Yamada, K. Matsubara, K. Nakahara, H. Takasu, *Phys. Status Solidi (a)* 180 (2000) 287.
- [7] A. Ohtomo, H. Kimura, K. Saito, T. Makino, Y. Segawa, H. Koinuma, M. Kawasaki, *J. Crystal Growth* 214/215 (2000) 284.
- [8] Single Crystal ZnO Substrate Specification, Eagle-Picher Technologies, 200 BJ Tunnell Blvd., Miami, OK 74354.
- [9] H.J. Ko, Y.F. Chen, S.K. Hong, H. Wenisch, T. Yao, D.C. Look, *Appl. Phys. Lett.* 77 (2000) 3761.
- [10] H. Kato, M. Sano, K. Miyamoto, T. Yao, *J. Crystal Growth* 237–239 (2002) 538.
- [11] D.C. Look, J.W. Hemsky, J.R. Sizelove, *Phys. Rev. Lett.* 82 (1999) 2552.
- [12] C.G. Van de Walle, *Phys. Rev. Lett.* 85 (2000) 1012.
- [13] F. Oba, S.R. Nishitani, S. Isotani, H. Adachi, I. Tanaka, *J. Appl. Phys.* 90 (2001) 824.
- [14] A.F. Kohan, G. Ceder, D. Morgan, C.G. Van de Walle, *Phys. Rev. B* 61 (2000) 15019.
- [15] K. Miyamoto, M. Sano, H. Kato, T. Yao, *Jpn. J. Appl. Phys.* 41 (2002) L1203.
- [16] D.C. Look, D.C. Reynolds, C.W. Litton, R.L. Jones, D.B. Eason, G. Cantwell, *Appl. Phys. Lett.* 81 (2002) 1830.
- [17] M.A.L. Johnson, S. Fujita, W.H. Rowland Jr., W.C. Hughes, J.W. Cook Jr., J.F. Schetzina, *J. Electron. Mater.* 25 (1996) 855.
- [18] P. Fons, K. Iwata, A. Yamada, K. Matsubara, S. Niki, *Appl. Phys. Lett.* 77 (2000) 1801.
- [19] K. Sakurai, M. Kanehiro, K. Nakahara, T. Tanabe, S. Fujita, S. Fujita, *J. Crystal Growth* 214/215 (2000) 92.
- [20] Y.F. Chen, H.J. Ko, S.K. Hong, T. Yao, Y. Segawa, *Appl. Phys. Lett.* 80 (2002) 1358.
- [21] H.J. Ko, T. Yao, Y.F. Chen, S.K. Hong, *J. Appl. Phys.* 92 (2002) 4354.
- [22] D. Sugihara, A. Kikuchi, K. Kusakabe, S. Nakamura, Y. Toyoura, T. Yamada, K. Kishino, *Jpn. J. Appl. Phys.* 39 (2000) L197.
- [23] F. Vigue, P. Vennegues, C. Deparis, S. Veizan, M. Laugt, J.P. Faurie, *J. Appl. Phys.* 90 (2001) 5115.
- [24] A. Usui, H. Sunakawa, A. Sakai, A.A. Yamaguchi, *Jpn. J. Appl. Phys.* 36 (1997) L899.
- [25] Y. Honda, Y. Iyechika, T. Maeda, H. Miyake, K. Hiramatsu, *Jpn. J. Appl. Phys.* 40 (2001) L309.
- [26] H. Amano, M. Iwaya, N. Hayashi, T. Kashima, M. Katsuragawa, T. Takeuchi, C. Wetzel, I. Akasaki, *MRS Internet J. Nitride Semicond. Res.* 4S1 (1999) G10.1.
- [27] H.M. Ng, D. Doppalapudi, T.D. Moustakas, *Appl. Phys. Lett.* 73 (1998) 821.
- [28] Y.F. Chen, S.K. Hong, H.J. Ko, V. Kirshner, H. Wenisch, T. Yao, K. Inaba, Y. Segawa, *Appl. Phys. Lett.* 78 (2001) 3352.
- [29] W.T. Read, *Philos. Mag.* 45 (1954) 775.
- [30] M. Sano, H. Kato, K. Miyamoto, T. Yao, *Jpn. J. Appl. Phys.* 42 (2003) L1050.